

# A 67- $\mu$ W Ultra-Low Power PVT-Robust MedRadio Transmitter

Somok Mondal and Drew A. Hall  
University of California San Diego, La Jolla, CA, USA

**Abstract**—A 400 MHz narrowband MedRadio transmitter for short-range communication is presented. A new technique for PVT-robust, calibration- and regulation-free synthesis of the RF carrier is reported based on generating poly-phasors at 50 MHz with no power overhead. This is accomplished using a passive polyphase filter directly integrated within a crystal oscillator followed by an  $8\times$  edge combiner to synthesize the RF carrier with  $-109$  dBc/Hz phase noise at 100 kHz offset. A dual supply, inverse class-E power amplifier is implemented for high efficiency at low output power ( $-17.5$  dBm). Open-loop operation permits aggressive duty-cycling ( $< 40$  ns start-up time). State-of-the-art ultra-low power is reported from a prototype BPSK transmitter fabricated in 22 nm CMOS FDX when operated from a 0.4/0.2 V supply consuming 67  $\mu$ W with 27% global efficiency.

**Keywords**—Crystal oscillator, edge combiner, IoT transmitter, low-power frequency synthesizer, MedRadio, wearable devices

## I. INTRODUCTION

The Internet-of-Things (IoTs) era is experiencing rapid growth with deployment of a wide variety of sensor nodes, most notably for healthcare monitoring and industrial automation. An important distinction from classic radios is that such IoT nodes only need to wirelessly communicate over short distances, typically  $\sim 1$ -2 meters, to reach a nearby data-aggregator (e.g., smartwatch, smartphone, etc.), as shown in Fig. 1(a). Owing to their autonomous and unobtrusive nature, enabling high deployment lifetimes through ultra-low power (ULP) operation is critical and often achieved through aggressive duty cycling.

Hence, simplistic transmitter topologies are preferred. In contrast to conventional radios, the power amplifier (PA) in a short-range radio is not the highest power consuming block due to the low output power,  $P_{out}$ . Instead, the frequency synthesizer or phase-locked loop (PLL) consumes a significant fraction of the overall transmitter power. The MedRadio/ISM band ( $\sim 400$  MHz) is widely used for the aforementioned applications due to its relatively low carrier frequency and considering the link distance [1]. To generate this RF carrier in an ULP manner, ring oscillator (RO)-based injection-locked clock multipliers (ILCMs) with small frequency multiplication factors ( $\sim 8$ - $12\times$ ) are regarded as the state-of-the-art [2–5].

Excellent low power performance using open-loop ILCMs has been reported in [2]. However, without a dedicated frequency tracking loop (FTL) or PLL to continuously set the oscillator frequency and ensure lock, these lead to an inevitable compromise in the robustness, especially since ROs are very sensitive to process, voltage, and temperature (PVT) variation. Henceforth, latter works have performed an initial frequency calibration [3–4] or used temperature compensation techniques [5], at the expense of higher power consumption. The former technique only accounts for static variations and suffers from slow start-up if calibration is needed each time. While dynamic temperature variation is addressed in the latter work, the RO

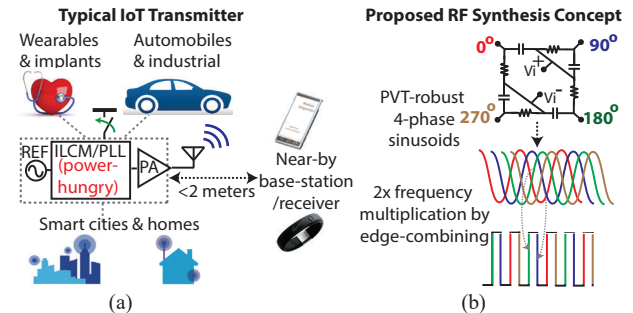


Fig. 1. (a) A typical IoT transmitter and applications. (b) Conceptual overview of the proposed technique with a  $2\times$  multiplier example.

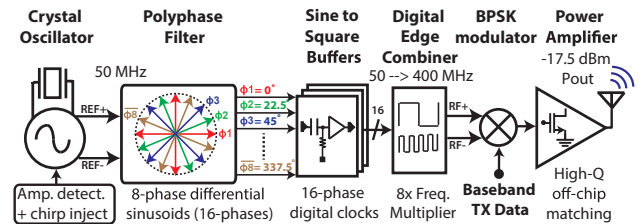


Fig. 2. Proposed MedRadio transmitter architecture.

sensitivity to supply voltage is not addressed. Dynamic voltage variation is important since IoT sensor nodes are often powered through energy harvesting, the design of which can be relaxed if imprecise voltage regulation and slow drift can be tolerated.

Towards this end, a new transmitter architecture is introduced to simultaneously realize ULP operation and ensure PVT robustness. Illustrated in Fig. 1(b), the key idea is to use a passive polyphase filter (PPF) to generate PVT insensitive, multiphase sinusoids that are subsequently used for frequency multiplication via edge combining. Fast start-up and a high-efficiency, low  $P_{out}$  inverse class-E PA are other key features of this work. The prototype 400 MHz narrowband MedRadio transmitter was fabricated in a 22 nm CMOS FDX process and achieves state-of-the-art performance.

## II. MEDRADIO TRANSMITTER ARCHITECTURE

The proposed transmitter architecture is shown in Fig. 2. A differential crystal oscillator (DXO) generates a 50 MHz reference frequency. An amplitude control loop controls the swing to minimize power and a chirp injector enables fast start-up. Similar to ILCMs, the small frequency multiplication factor ( $8\times$ ) needed for the MedRadio carrier frequency is leveraged to synthesize the 400 MHz carrier from the 50 MHz reference without a PLL. This is done with the aid of a 16-phase passive RC PPF integrated within the DXO. The polyphase sinusoids at 50 MHz are generated in a PVT-insensitive, calibration-free manner and, importantly, incur no additional power overhead. It may be noted that integrating a PPF with a bulk acoustic wave

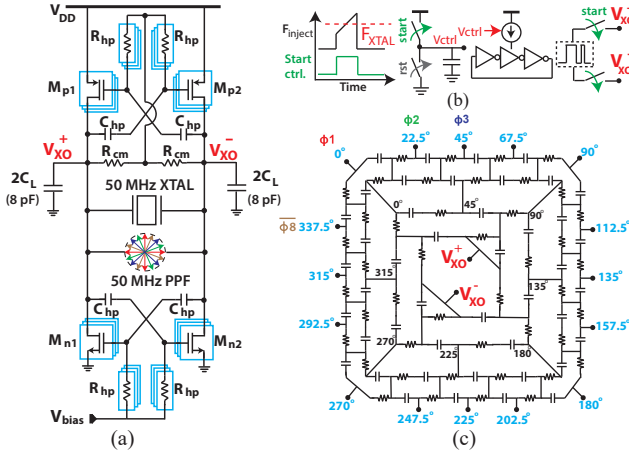


Fig. 3. Implementation of (a) differential current-reuse crystal oscillator, (b) chirp injector, and (c) 16-phase, 4-ring passive RC polyphase filter.

(BAW) resonator was reported in [6] to generate 4-phases for quadrature phase shift keying (QPSK) modulation. In this work, the 16-phases are buffered and processed by a digital edge combiner for RF carrier synthesis. The resulting differential RF carrier is binary phase-shift keying (BPSK) modulated and transmitted via an inverse class-E PA with an off-chip matching network and  $P_{\text{out}}$  of -17.5 dBm.

### III. CIRCUIT IMPLEMENTATION

#### A. Current-reuse Differential Crystal Oscillator

The proposed PPF-based technique requires a differential reference at 50 MHz generated by the digitally current-tunable DXO, as shown in Fig. 3(a). The oscillator uses cross-coupled differential pairs that are ac-coupled by 200 fF capacitors,  $C_{\text{hp}}$ . This prevents latch-up due to the high dc impedance of the crystal resonator. Furthermore, the biasing resistors,  $R_{\text{hp}}$ , dampen unwanted low-frequency parasitic oscillation modes due to the ac-coupling. Both the ac-coupling and resistive biasing techniques are incorporated from [7]. The ac-coupling also provides an opportunity to use complementary cross-coupled transistors. A current-reuse structure with  $2\times$  transconductance  $G_m$  boosting is realized to improve the power efficiency. The NMOS differential pairs are biased to set the desired current whereas the PMOS devices are self-biased by the output common-mode voltage, as shown in Fig. 3(a).

Arrays of switchable  $G_m$  blocks provide the digital control feature. A Schmitt-trigger-based amplitude detector regulates the output amplitude and minimizes the power consumption for a one-time setting of the DXO. It may be noted that the criteria to avoid parasitic oscillations depends on the  $G_m R_{\text{hp}}$  product. Hence,  $R_{\text{hp}}$  is tuned in tandem with  $G_m$ . The overall transmitter duty-cycling is limited by the crystal oscillator start-up time. To enable fast start-up, chirp injection is used. As shown in Fig. 3(b), a current starved voltage-controlled oscillator (VCO) is controlled by a ramp to inject frequencies swept across the 50 MHz reference frequency at start-up. The crystal is an Abracon ABM10W with a 4 pF load capacitance,  $C_L$ , and an 8.4  $\Omega$  equivalent series resistance (ESR).

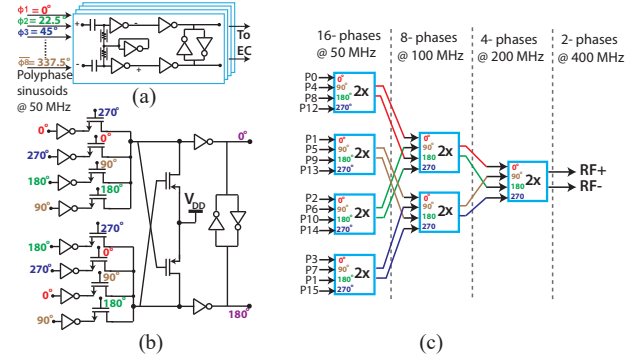


Fig. 4. Implementation of (a) PPF output buffer, (b)  $2\times$  frequency multiplier, and (c)  $8\times$  frequency multiplier via edge combining.

#### B. Passive RC Polyphase Filter

The RC PPF used to generate the 8-phase differential sinusoids is shown in Fig. 3(c). The choice of  $R$  and  $C$  values impacts the phase noise where a larger  $C$  or charge swing is associated with lower phase noise. Each PPF unit resistor,  $R$ , is 37 k $\Omega$  while each unit capacitor,  $C$ , is 85 fF and loads the DXO negligibly considering its own  $C_L$ . An additional fourth outer balanced RC ring in the PPF performs phase averaging and maintains symmetry when the outputs are equally loaded.

The PPF robustness is well known. For a 4-phase PPF it can be shown that a small  $\Delta RC$  change in the  $RC$  product (e.g., due to PT variations) results in each phasor being shifted equally by  $\Delta RC/2RC$  and attenuated [8]. The generated phasors incur no frequency error and exhibit no voltage dependence. Systematic imbalance and mismatch do result in spurs at multiples of the reference frequency; however, good carrier-to-spur ratio (CSR) is maintained due to the harmonic suppression of the PA.

#### C. RF Synthesis by Edge Combining and Data Modulation

The differential PPF outputs are buffered using ac-coupled inverters that also convert the sinusoids to square wave digital signals, as shown in Fig. 4(a). The edge combining is performed with transmission gate logic based ULP digital circuits. Implementation of a  $2\times$  multiplier block is shown in Fig. 4(b). Multiple such blocks arranged in a tree-like structure, as shown in Fig. 4(c), are used to synthesize the differential 400 MHz RF carrier. BPSK modulation is realized with a phase mux controlled by the baseband data.

#### D. Power Amplifier

A generic PA, as shown in Fig. 5(a), comprises a resonant network based on the PA's class and a matching network to transform the antenna load,  $R_L$ , by a factor  $N$  to an impedance  $R_p = NR_L$  and thereby set a desired  $P_{\text{out}} \propto V_{\text{DD}}/R_p$ , where  $V_{\text{DD}}$  is the supply voltage. For most PA classes, the low  $P_{\text{out}}$  (< 20  $\mu\text{W}$ ) requirement translates to  $N > 1$  or  $R_p$  to be a few k $\Omega$ s as opposed to a few  $\Omega$ s in a conventional high  $P_{\text{out}}$  PA. This causes significant losses in the matching network [9] that severely limits the efficiencies of short-range PAs. In this work, a class-E PA with a shunt inductor or inverse class-E [10] with

$$P_{\text{out}} = \frac{8}{\pi^2(\pi^2 + 4)} V_{\text{DD}}^2 / R_p = 0.058 V_{\text{DD}}^2 / R_p \quad (1)$$

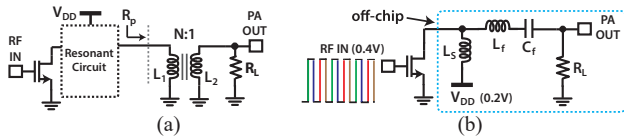


Fig. 5. Implementation of a (a) generic PA and (b) inverse class-E PA.

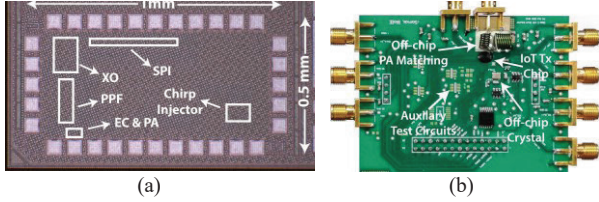


Fig. 6. Annotated (a) chip micrograph and (b) photograph of the printed circuit board (PCB).

is implemented. A dual supply scheme with a PA  $V_{DD}$  of 0.2 V, half of the 0.4 V core, is used. Thus, a low  $P_{out}$  is readily delivered, eliminating the need for any impedance transformation ( $N = 1$ ). High- $Q$  off-chip 50-130 nH Coilcraft inductors are used for the implementation shown in Fig. 5(b).

#### IV. MEASUREMENT RESULTS

This MedRadio transmitter was fabricated in a 22 nm CMOS FDX process and occupies an active area of 0.03 mm<sup>2</sup>. The DXO, edge combiner, and PA drivers are operated at 0.4 V while the PA is operated at 0.2 V. A chip micrograph and a photograph of the printed circuit board implementation with the off-chip components used are shown in Fig. 6.

The key novelty of this work is the PVT-robust frequency synthesis and hence relevant measurements are discussed first. The  $8\times$  frequency multiplication functionality remained consistent over a wide temperature range (-30 to 90 °C). The associated frequency variation of the generated 400 MHz RF carrier measured over multiple chips ( $n = 4$ ) is plotted in Fig. 7(a) and is less than 20 ppm/°C, validating the stability of the reference generated from the DXO with integrated PPF. Excellent supply insensitivity is maintained with less than 2 ppm/V frequency variation when the supply was swept from 0.35 to 0.6 V, as shown in Fig. 7(b). It may be noted that this is a significant benefit compared to ILCMs that suffer from poor line sensitivity and need re-calibrating with voltage drift. The measured phase noise of the RF carrier and the reference DXO are shown in Fig. 8. A phase noise of -109 dBc/Hz at 100 kHz offset of the RF carrier was measured at room temperature. This remains consistent over temperature, as shown in Fig. 8, demonstrating the temperature robustness. The spectrum of an unmodulated transmitter output is shown in Fig. 9 along with overlaid plots at different temperatures for comparison. The CSR is better than 40 dB across temperature. Overall, the MedRadio regulations which require a 100 ppm/°C frequency accuracy over 0 to 55 °C and attenuation of out-of-band spurs by 20 dB are met with significant margin.

The spectrum of the data transmitted and received using 400 MHz quarter-wave whip antennas at 1-meter separation is shown in Fig. 10. The error vector magnitude (EVM) is 7.34% rms at a 1 Mbps data-rate. The open-loop operation of the frequency synthesizer permits aggressive duty-cycling

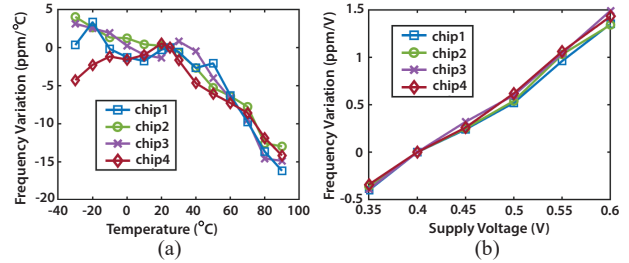


Fig. 7. Measured frequency variation of the synthesized RF carrier versus (a) temperature and (b) supply voltage.

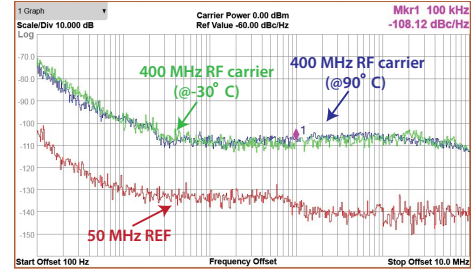


Fig. 8. Measured phase noise of the 50 MHz DXO and the synthesized 400 MHz RF carrier for the temperature endpoints of -30 and 90 °C.

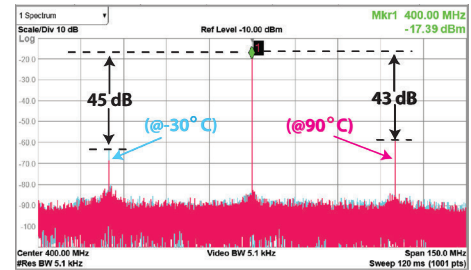


Fig. 9. Measured unmodulated transmitter output spectra at room temperature and temperature endpoints of -30 and 90 °C.

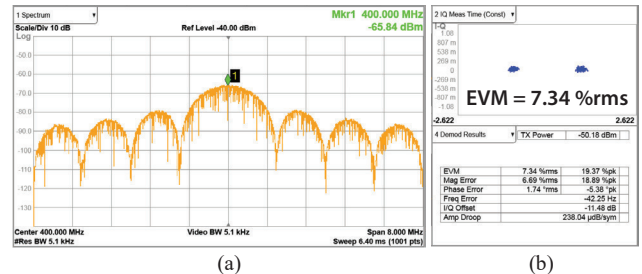


Fig. 10. Measurements of BPSK modulated (a) received spectra and (b) demodulated constellation at 1 Mbps data-rate.

(considering only the frequency multiplier and PA). Contrary to ILCMs where a RO needs to first have stable oscillation set-up and then wait to get locked, the start-up with the proposed technique is instantaneous, in theory. The settling time upon applying a ramp on the supply is shown in Fig. 11(a) and confirms start-up within  $\sim 10$  cycles of the RF carrier ( $< 40$  ns). A power-efficient overall shutdown feature for sensor node is also supported by the fast DXO start-up. With a chirp-injection settling time of 150  $\mu$ s, shown in Fig. 11(b), compared to an otherwise more than 3 ms slow settling, is achieved. Finally, this work is summarized in Table 1 and compared to prior relevant short-range transmitters.

Table 1. Comparison of Short-Range Narrowband Transmitters.

	[2] JSSC'11	[3] TBioCAS'13	[11] RFIC'13	[3] JSSC'14	[12] RFIC'15	[13] ISSCC'19	This work	
Supply (V)	0.7	0.6	0.7/1.2	0.8	1.2	1.2	0.4/0.2	
Technology (nm)	90	90	130	65	130	65	22 FDX	
Active Area (mm <sup>2</sup> )	0.04	0.06	0.41	0.08	0.29	0.49	0.03	
Frequency (MHz)	400	400	405	900	915	2400	400	
Frequency Synthesizer								
Phase Noise (dBc/Hz)	-105.2 @0.3 MHz	-87.9 @0.3 MHz	-69 @0.1 MHz	-100 @1 MHz	-100.2 @1 MHz	-118 @1 MHz	-109 @0.1 MHz	
Power (μW)	<78*	-	72	538	224	-	10	
Freq. Multiplier	9×	25×	25×	9×	60×	1×	8×	
CSR (dB)	44	22	48	56	-	-	45	
Power Amplifier								
P <sub>out</sub> (dBm)	-17	-17	-16	-15	-18	-8.4	-17.5	
PA Efficiency (%)	30	-	33	9	12.5	-	40	
Power (μW)	<78*	-	80	351	110	-	44	
Crystal Oscillator/Reference								
Frequency (MHz)	45	16	-	100	16	16	50	
Power (μW)	<12	External	External	External	32	External	13	
Transmitter								
Topology	ILRO+EC-PA	2-step ILRO	PLL+PA	ILRO+PA	PLL+PA	PO.+PLL calib.	XO-PPF+EC+PA	
Modulation	BFSK	OOK	BFSK	QPSK	FSK	GFSK	BPSK	
Data-rate (Mbps)	0.2	1	0.08	10	3	1	1	
Energy/bit (pJ/bit)	450	160	2375	130	122	606	67	
Settling Time (ns)	250 <sup>1</sup>	250 <sup>1</sup>	-	88 <sup>1</sup>	-	-	40 <sup>1</sup>	150 μs <sup>2</sup>
PVT-robust?	P× V× T×	P✓ V× T×	P✓ V✓ T✓	P✓ V× T×	P✓ V✓ T✓	P✓ V✓ T✓	P✓ V✓ T✓	
Calibration reqd.?	✓	✓	×	✓	×	×	× <sup>#</sup>	
Total Power (μW)	90	160	190	1,300	367	606	67	
Global Efficiency%	22	16	13	4	12	24	27	

Global Efficiency% =  $P_{out} / Total\ Power$ ; ILRO: Injection-locked RO; PO: Power oscillator; EC: edge combiner; XO: crystal oscillator;  
<sup>#</sup>XO calibrated once but not repeated for dynamic variations; Start-up time <sup>1</sup>w/o XO and <sup>2</sup>w/ XO; <sup>1</sup>EC and PA are merged and reported together

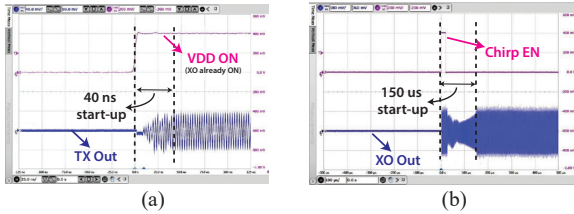


Fig. 11. Measured start-up transients for (a) transmitter and (b) DXO.

## V. CONCLUSION

An ultra-low power MedRadio transmitter is presented. Robustness of the RF frequency synthesis is enabled with the aid of a passive PPF that is integrated within the DXO and hence has no power overhead and doesn't require any calibration. Although the DXO is trimmed once for amplitude regulation, re-calibrations to account for dynamic VT variations are not needed. The proposed concept can also be extended for higher frequency or smaller area applications using film bulk acoustic resonators (FBARs). In this work, at a data-rate of 1 Mbps, an energy efficiency of 67 pJ/bit is achieved. Aggressive duty-cycling of 40 ns is supported. A class-E inverse PA operates with a 40% efficiency delivering a low output power of -17.5 dBm. To the authors' knowledge, a best-reported power consumption of 67 μW and a global efficiency of 27% for short-range narrowband transmitters is achieved.

## ACKNOWLEDGEMENTS

This work was supported in part by the UCSD Center for Wireless Communications. The authors thank Li Gao for technical guidance and Global Foundries for chip fabrication.

## REFERENCES

- J. L. Bohorquez, et al., "A 350 μW CMOS MSK Transmitter and 400 μW OOK Super-Regenerative Receiver for Medical Implant Communications," *IEEE JSSC*, vol. 44, pp. 1248–1259, Apr. 2009.
- J. Pandey, et al., "A Sub-100 μW MICS/ISM Band Transmitter Based on Injection-Locking and Frequency Multiplication," *IEEE JSSC*, vol. 46, no. 5, pp. 1049–1058, May 2011.
- X. Liu, et al., "A 13 pJ/bit 900 MHz QPSK/16-QAM Band Shaped Transmitter Based on Injection Locking and Digital PA for Biomedical Applications," *IEEE JSSC*, vol. 49, no. 11, pp. 2408–2421, Nov. 2014.
- C. Ma, et al., "A Near-Threshold, 0.16 nJ/b OOK-Transmitter With 0.18 nJ/b Noise-Cancelling Super-Regenerative Receiver for the Medical Implant Communications Service," in *IEEE TBioCAS*, vol. 7, no. 6, pp. 841–850, Dec. 2013.
- S. Mondal, et al., "A 107 μW MedRadio Injection-Locked Clock Multiplier with a CTAT-biased 126 ppm/°C Ring Oscillator," in *IEEE CICC*, 2019, pp. 1–4.
- P. Nadeau, et al., "Single-BAW multi-channel transmitter with low power and fast start-up time," in *ESSCIRC 2017*, pp. 195–198.
- Y. Chang, et al., "A Differential Digitally Controlled Crystal Oscillator With a 14-Bit Tuning Resolution and Sine Wave Outputs for Cellular Applications," *IEEE JSSC*, vol. 47, no. 2, pp. 421–434, Feb. 2012.
- B. Razavi, "RF Microelectronics (2nd Edition)", Prentice Hall 2011.
- S. Iguchi, et al., "Design Method of Class-F Power Amplifier With Output Power of 20 dBm and Efficient Dual Supply Voltage Transmitter," *IEEE TCAS-I*, vol. 61, no. 10, pp. 2978–2986, Oct. 2014.
- M. Kazimierzczuk, "Class E tuned power amplifier with shunt inductor," *IEEE JSSC*, vol. 16, no. 1, pp. 2–7, Feb. 1981.
- K. Natarajan, et al., "A PLL-based BFSK transmitter with reconfigurable and PVT-tolerant class-C PA for MedRadio & ISM (433MHz) standards," in *IEEE RFIC Symposium*, 2013, pp. 67–70.
- M. S. Jahan, et al., "A low-power FSK/OOK transmitter for 915 MHz ISM band," in *IEEE RFIC Symposium*, 2015, pp. 163–166.
- Y. Shi, et al., "28.3 A 606μW mm-Scale Bluetooth Low-Energy Transmitter Using Co-Designed 3.5×3.5mm<sup>2</sup> Loop Antenna and Transformer-Boost Power Oscillator," in *IEEE ISSCC*, 2019, pp. 442–444.